Bridge Piers with Structural Fuses and Bi-Steel Columns. II: Analytical Investigation

Samer El-Bahey[1] and Michel Bruneau, F.ASCE[2]

Abstract: This paper presents the results of an analytical investigation conducted to replicate experimentally obtained behavior, and better understand the behavior of the proposed structural fuse concept for bridges that is presented in a companion paper. First, a steel plate shear link (SPSL) proposed as a new type of structural fuse is described. Equations are derived to define its shear-moment interaction equation, to determine some of its critical design parameters, and to quantify the link ductility, lateral stiffness and strength. Strengths and stiffnesses equations are developed using free-body diagrams (FBDs) for the tested systems as a convenient simple design tool. Finite-element models (FEM) are developed by using the finite-element software package ABAQUS/explicit to validate the proposed SPSL concept, and then to replicate the full range of results obtained from the experiments. Comparisons between the analytical and experimental results are conducted to highlight the differences in behavior among all tested specimens. The simple numerical equations correctly represent the expected strengths and stiffnesses of the fuse systems. Further, the results obtained from the ABAQUS model accurately captured the global behavior of the system, and provided valuable insight into individual fuse behavior. **DOI: 10.1061/(ASCE)BE.1943-5592.0000236.**

CE Database subject headings: Bracing; Plates; Seismic effects; Finite-element method; Bridges; Steel columns.

Author keywords: Structural fuses; Buckling restrained braces; Steel plate shear links; Seismic; Bridges; Finite-element analysis.

Introduction

The concept of designing sacrificial elements to dissipate seismic energy whereas preserving the integrity of the structure's other main components is known as the structural fuse concept. Few implementations of the structural fuse concept have been rigorous in emphasizing easy replaceability of the sacrificial elements and absence of damage to the primary load-resisting structural system. An experimental investigation, presented in a companion paper (El-Bahey and Bruneau 2011), was conducted to validate the structural fuse concept as part of a proposed multicolumn accelerated bridge construction (ABC) pier application to keep the columns elastic, and concentrate seismic energy dissipation in replaceable fuses. Different types of fuses were investigated [buckling restrained braces (BRBs) and steel plate shear links (SPSLs)] to compare their respective performance in the ABC bridge bents.

This paper presents the analysis and modeling of the experimental specimens to replicate the observed behavior during testing. First, the proposed SPSL structural fuse (shown in Fig. 1), which consists of a steel plate restrained from out-of-plane buckling, is presented. Out-of-plane buckling can be prevented by using various types of material providing sufficient lateral stiffness and strength to counter the out-of-plane motion of the plate. For example, concrete encasement and an unbonding material to reduce friction between the steel and the concrete encasement could be used; sleeves of thick steel plates also could be used for the same purpose. Here, fiber-glass panels were used for ease of construction and because of their light weight. The steel plate was designed to yield in shear, at a stress equal to $0.6\sigma_y$, dissipating the seismic energy. Equations for the expected strengths and stiffnesses of the total proposed systems, formulated using free-body diagrams (FBDs), are then presented to investigate the effectiveness of such simple design equations to estimate these values. Then, finite-element models (FEM) are developed by using the commercially available software package ABAQUS/explicit [Hibbett, Karlsson, and Sorensen (HKS) 2005], to investigate behavior of the proposed SPSL concept and to capture in more detail the experimentally observed behavior of the total system. Comparison between the experimental and analytical results obtained from both approaches are presented.

Steel Plate Shear Link

Three types of plastic mechanisms can develop in laterally restrained links, regardless of the shape of the cross section; depending on link length, these are:

- Flexural links (pure flexural yielding) developing full plastic moment hinges, M_p, at the ends of the links and a corresponding shear force less than the full plastic shear force, V_p. These links dissipate energy by flexural plastic rotation.
- Shear links (pure shear yielding) developing full plastic shear force, V_p, over the entire length of the link, with corresponding moments at their ends less than the plastic moment reduced to account for the presence of shear, M_p^r. These links dissipate energy by shear plastic rotation.
- Intermediate links, which are links yielding in both flexure and shear, in which, one yielding mode develops after the other mode strain hardens.

Various experimental studies of link behavior by previous researchers reported that shear links exhibit the most stable and ductile cyclic behavior. For example, for the type of links typically

[1]Structural Engineer, Stevenson & Associates, Phoenix, AZ 85395 (corresponding author). E-mail: selbahey@gmail.com

[2]Professor, Dept. of Civil, Structural, and Environmental Engineering, State Univ. of New York at Buffalo, Buffalo, NY 14260.

Note. This manuscript was submitted on August 12, 2010; approved on February 22, 2011; published online on February 24, 2011. Discussion period open until June 1, 2012; separate discussions must be submitted for individual papers. This paper is part of the ***Journal of Bridge Engineering***, Vol. 17, No. 1, January 1, 2012. ©ASCE, ISSN 1084-0702/2012/1-36–46/$25.00.

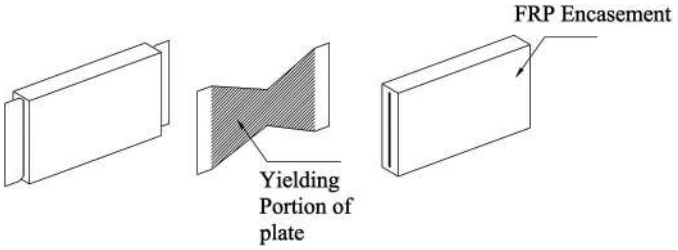

Fig. 1. Proposed link illustration

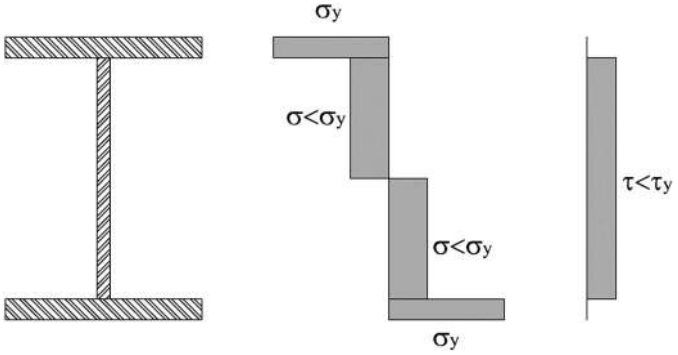

Fig. 2. Assumed normal and shear stress distribution

used in eccentrically braced frames (EBFs), Kasai and Popov (1986a, 1986b) reported that shear links (short links) can develop large inelastic shear strains over the entire link length, and that well-detailed links can sustain plastic rotations of 0.1 rad without failure; whereas Engelhardt and Popov (1989) reported that flexural links (long links), owing to the high bending strains that develop at their ends, can only sustain inelastic deformations that corresponds to a plastic rotation of 0.02 rad (about 1/5 that of a shear link).

Given that the ultimate failure mode for shear links is inelastic web shear buckling, to delay that failure mode in EBFs, Kasai and Popov (1986a) recommended adding vertical stiffeners, and provided simple rules to calculate the stiffeners spacing as a function of the maximum inelastic link rotation. For the type of link proposed here, web shear buckling is overcome by wrapping the steel plate with a material that has sufficient lateral stiffness and strength to prevent out-of-plane buckling of the link's steel plate.

Given that the proposed SPSL link varies from those used in conventional eccentrically braced frames (EBF), it is necessary for design purposes and behavior study to formulate shear-moment interaction equations for the proposed element. Shear-moment interaction equations have been studied previously for different hybrid steel sections; a lower bound interaction equation (ASCE 1971) can be applied by using the stress distribution shown in Fig. 2. Berman and Bruneau (2005) used a similar stress distribution to derive the interaction equation for shear links that have hybrid tubular cross sections.

For the new type of shear link proposed in this paper, a similar assumed stress distribution is chosen, as shown in Fig. 3. In this approach, shear yielding is assumed to occur over a depth of y_o over the entire length of the link. Becasuse the link is in double curvature, the midlength point along the link is in pure shear, and moment increases from zero at this point to a value at the link ends equal to the plastic shear strength. The slope, θ, of the link edges must therefore vary linearly (like the moment diagram) to provide this needed moment strength. From that basis, the following equations can be derived

$$V = \tau t y_0 = \frac{\sigma}{\sqrt{3}} t y_0 \tag{1}$$

$$M^V = \sigma_y y_1 t (y_0 + y_1) + \sigma \frac{t y_0^2}{4} \tag{2}$$

in which V = existing shear force along for section A-A; M^V = corresponding moment in presence of shear force for section B-B; and σ_y = yield stress of the plate.

For comparison, the full plastic moment and full plastic shear can be derived as:

$$M_p = \sigma_y \frac{t(y_0 + 2y_1)^2}{4} \tag{3}$$

$$M_{pr} = \sigma_y y_1 t (y_0 + y_1) \tag{4}$$

$$V_p = \frac{\sigma_y}{\sqrt{3}} t y_0 \tag{5}$$

in which M_p = full plastic moment of section B-B; M_{pr} = reduced plastic moment of section B-B attributable to the presence of full plastic shear; and V_p = full plastic shear of section B-B.

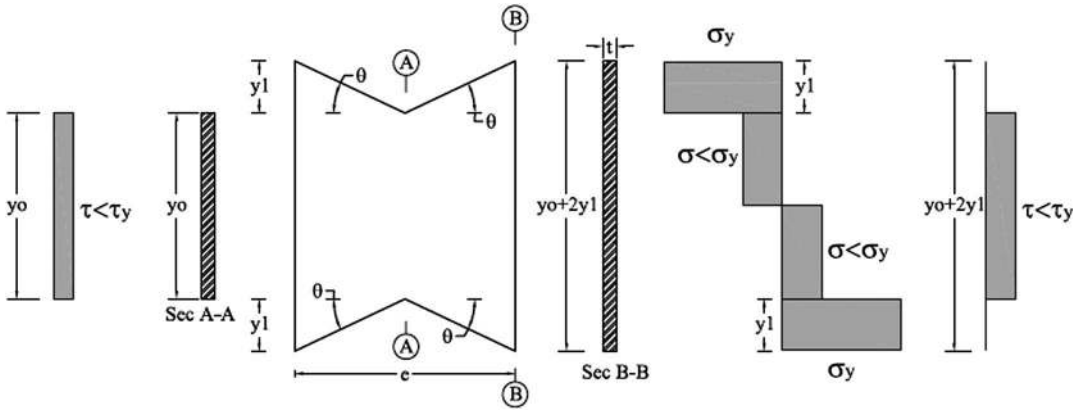

Fig. 3. Assumed stress distribution in mid and end plate

By using the previously defined equations, an interaction equation for the proposed element can be expressed as:

$$\frac{M^V}{M_p} = \frac{4y_1(y_o + y_1)}{(y_o + 2y_1)^2} + \left(\frac{4}{t(y_o + 2y_1)^2} \sqrt{1 - \left(\frac{V}{V_P}\right)^2} \right) \tag{6}$$

At $V = V_p$, M^V would be equal to M_{Pr}.

Shear links can be defined as a function of the link length, e, in terms of the balanced length, e^*, which is the point when the transition from flexural to shear yielding occurs. The balanced link length can be calculated by considering the equilibrium of the free-body diagram of the link as:

$$e^* = \frac{2y_o}{\sqrt{3}\tan^2\theta}(1 - \sqrt{3}\tan\theta) \tag{7}$$

Another important factor governing the behavior of the link is the link edge angle, θ. Whereas changing the link length changes the behavior of the link from shear to flexure, changing the link edge angle, θ, changes the way yielding propagates in the plate.

For yielding to develop in the plate where flexural and shear yielding occurs simultaneously, geometry of the link is defined by the balanced link edge angle, θ_b, which can be obtained from the equilibrium of the balanced link length shown in Fig. 4

$$\tan^2\theta_b + \frac{2y_0}{e}\tan\theta_b - \frac{2y_0}{e\sqrt{3}} = 0 \tag{8}$$

from which values of θ_b can be found with respect to y_o/e, itself an expression of the aspect ratio of the link with large values of y_o/e corresponding to deeper links.

One of the most important desired characteristics of this proposed SPSL is the ability to dissipate by hysteretic behavior the seismic energy of the earthquake, without introducing ductility in any other parts of the bridge piers. Expressions for the maximum ductility that a SPSL withstands were therefore developed in terms of the global dimensions of the bridge bent and the dimensions of the link itself.

The value of the link rotation, γ, in terms of the structure deformation can be derived from the geometry of the structure. No relative deformation is assumed to occur in the bridge pier segments adjacent to the links, as they are considered rigid compared to the links. The link connection parts also are assumed to remain elastic; their relative deformations are ignored as they are relatively small compared to the plastic deformation in the links. The structure deformation can be considered by superposition of two effects, rotation of the bridge piers and relative vertical displacement between the bridge piers, and is found to be equal to:

$$\gamma_{\text{tot}} = \frac{\Delta L}{he} + \frac{\delta}{e} = \frac{1}{e}\left(\frac{\Delta L}{h} + \delta\right) \tag{9}$$

in which Δ and h are the lateral displacement and height, respectively, at which the SPSL is installed between the bridge columns; L = spacing between the bridge columns; and δ = relative vertical displacement between the bridge piers.

Because the purpose of the SPSL is to introduce ductility to the system to dissipate the seismic energy without introducing any plastic deformation to the piers, and because the amount of plastic rotation of the SPSL is tied to the drift of the pier as mentioned, it is necessary to limit drift not to exceed the columns yield drift, Δ_{yf}, so that the columns remain elastic. Consequently, the maximum amount of plastic rotation produced by the SPSL is limited to:

$$\gamma_{\max} = \frac{1}{e}\left(\frac{\Delta_{yf} L}{h} + \delta\right) \tag{10}$$

To find the value of the link ductility, the maximum SPSL rotation is divided by the yield SPSL rotation, γ_y, which is found as:

$$\gamma_y = \frac{\tau_y}{G} \tag{11}$$

in which τ_y = yield shear stress of the SPSL; and G = shear modulus, from which the value of the SPSL; ductility, μ_{link}, can be found as:

$$\mu_{\text{link}} = \frac{\gamma_{\max}}{\gamma_y} = \frac{G}{e\tau_y}\left(\frac{\Delta_{yf} L}{h} + \delta\right) \tag{12}$$

Plastic Analysis

The contribution of the fuses to the strength and elastic lateral stiffness of the total system can be calculated by finding the value of the seismic lateral load resisted by the link divided by the lateral displacement of the bridge bent at the onset of yielding of the fuses. To illustrate this, a bridge bent consisting of two columns is shown in Fig. 5, in which the columns maximum strength, V_{Df}, can be calculated from the following equation:

$$V_{Df} = \frac{4M_P}{H_{\text{tot}}} \tag{13}$$

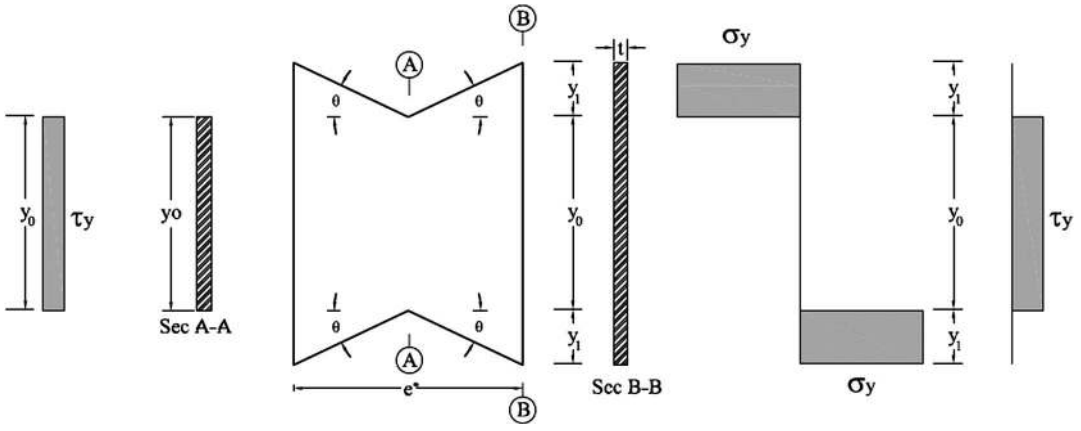

Fig. 4. Assumed stress distribution at balanced link edge angle

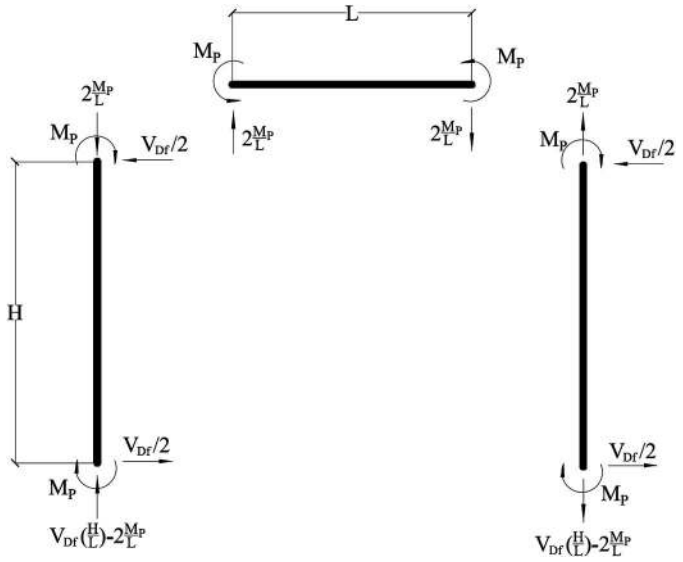

Fig. 5. Bridge bent consisting of two columns

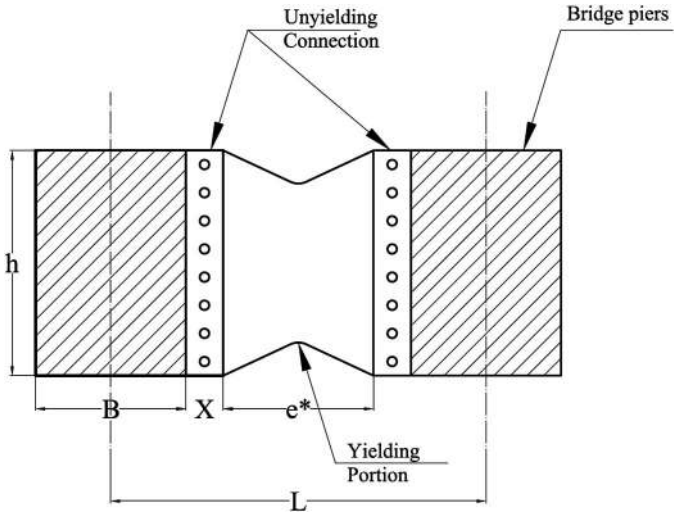

Fig. 7. Typical steel plate shear link introduced between two bridge column segments

in which H_{tot} = total height of the columns; and M_p = plastic moment of the columns.

First, the columns effective lateral stiffness, K_{eff}, can be calculated from the following equation, assuming that the top and bottom of columns do not rotate:

$$K_{\text{eff}} = \frac{24EI_{\text{eff}}}{H_{\text{tot}}^3} \tag{14}$$

in which I_{eff} = cracked moment of inertia of the columns; and E = its modulus of elasticity.

Fig. 6 shows a FBD of one of the columns after adding one restrained SPSL, from which the maximum system base shear, V_{Dt}, can be calculated by taking the moment around the base of the column as:

$$V_{Dt} = \frac{4M_P}{H_{\text{tot}}} + \frac{\sigma_y}{\sqrt{3}} t y_o \left(\frac{e+2X}{H_{\text{tot}}}\right) \tag{15}$$

It can be seen that the first term of the equation represents the maximum bare frame shear strength, from which it is concluded

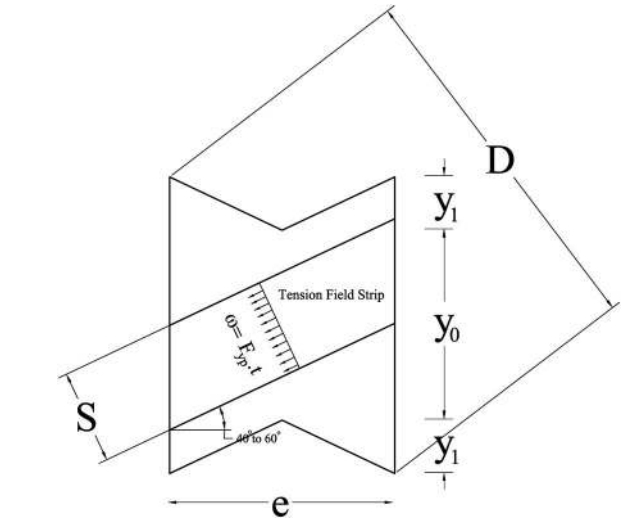

Fig. 8. Forces acting on steel plate shear link after initiation of buckling

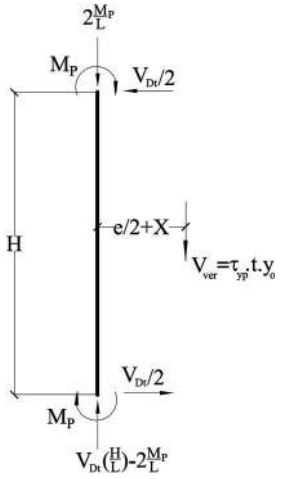

Fig. 6. Free-body diagram of column with steel plate shear link (with restraints)

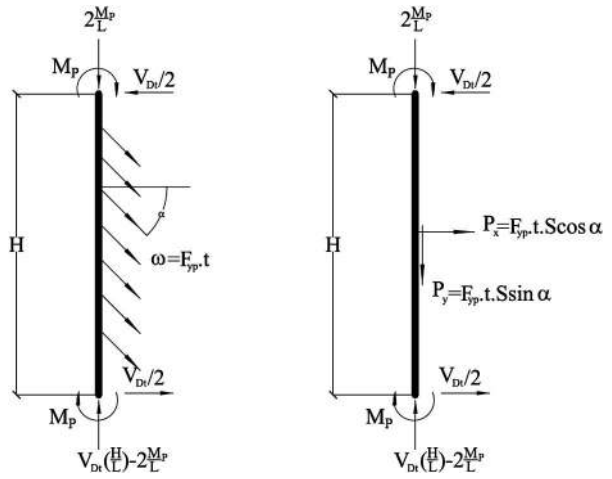

Fig. 9. Free-body diagram of column with steel plate shear link (no restraints)

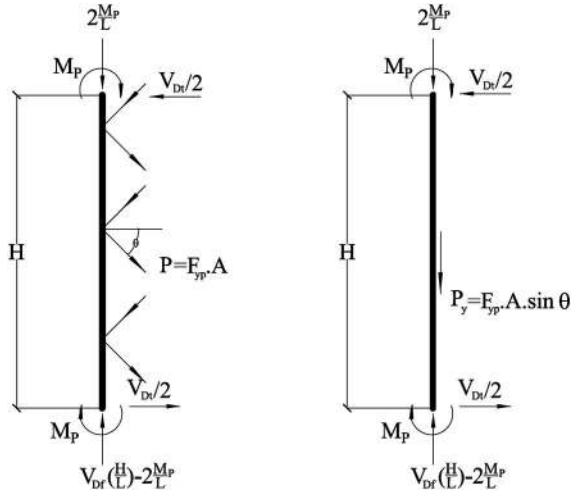

Fig. 10. Free-body diagram of a single column with buckling restrained braces

that the contribution of one laterally restrained SPSL to the maximum base shear strength, V_{DS}, is the second term of the equation. The total base shear attributed to adding multiple SPSLs could be calculated by multiplying the base shear contribution of the SPSL by the number of added links, n.

The elastic lateral stiffness contribution of a single SPSL to the total system can be written as:

$$K_b = \frac{Gty_0(B+2X)(e+2X)}{eH_{\text{tot}}^2} \tag{16}$$

in which K_b = contribution of SPSL to the lateral stiffness of the two-column bridge bent; y_o = height of the SPSL mid part; t = SPSL thickness; B = column width; X = unyielding length of the SPSL; and e = link length as shown in Fig. 7.

Again, the total elastic stiffness attributed to adding multiple SPSLs could be calculated by multiplying the elastic stiffness contribution of the SPSL by the number of added links. When the SPSLs are not restrained against out-of-plane motion, tension field action develops in the links after buckling occurs owing to inherent initial imperfections. This buckling results in a decreased contribution of the links to the lateral strength and secant stiffness of the total system. Fig. 8 shows a diagram of the forces acting in a SPSL attriubutable to the tension field action. The strip width, S, is assumed to be equal to $1/3$ of the total width, D. This is an assumption on the basis of the FEM results for the SPSLs, as it was observed that the tension field in the plates develop in a strip of approximately $1/3$ of the total width, inclined at an angle, α, ranging from 40 to 60 ° (owing to interaction of shear and flexure stresses).

Fig. 9 shows a FBD of one of the columns with laterally unrestrained SPSLs, from which the maximum system base shear, V_{Dt}, can be calculated by taking the summation of the vertical forces as:

$$V_{Dt} = \frac{4M_P}{H_{\text{tot}}} + n\sigma_y tS\left(\frac{L}{H_{\text{tot}}}\right)\sin\alpha \tag{17}$$

Again, because the first term of the equation represents the maximum bare frame shear strength, the contribution of the laterally unrestrained SPSLs to the maximum shear strength, V_{DS}, is therefore given by the second term in the equation.

The value of the elastic lateral stiffness contribution of a single unrestrained SPSL to the total system elastic lateral stiffness can be calculated as:

$$K_b = \sqrt{3}G\left(\frac{tS(B+2X)L\sin\alpha}{H_{\text{tot}}^2 e}\right) \tag{18}$$

Fig. 10 shows the free-body diagram for a single column with BRB fuses, from which the maximum system base shear, V_{Dt}, can be calculated by taking sum of the forces along the vertical axis:

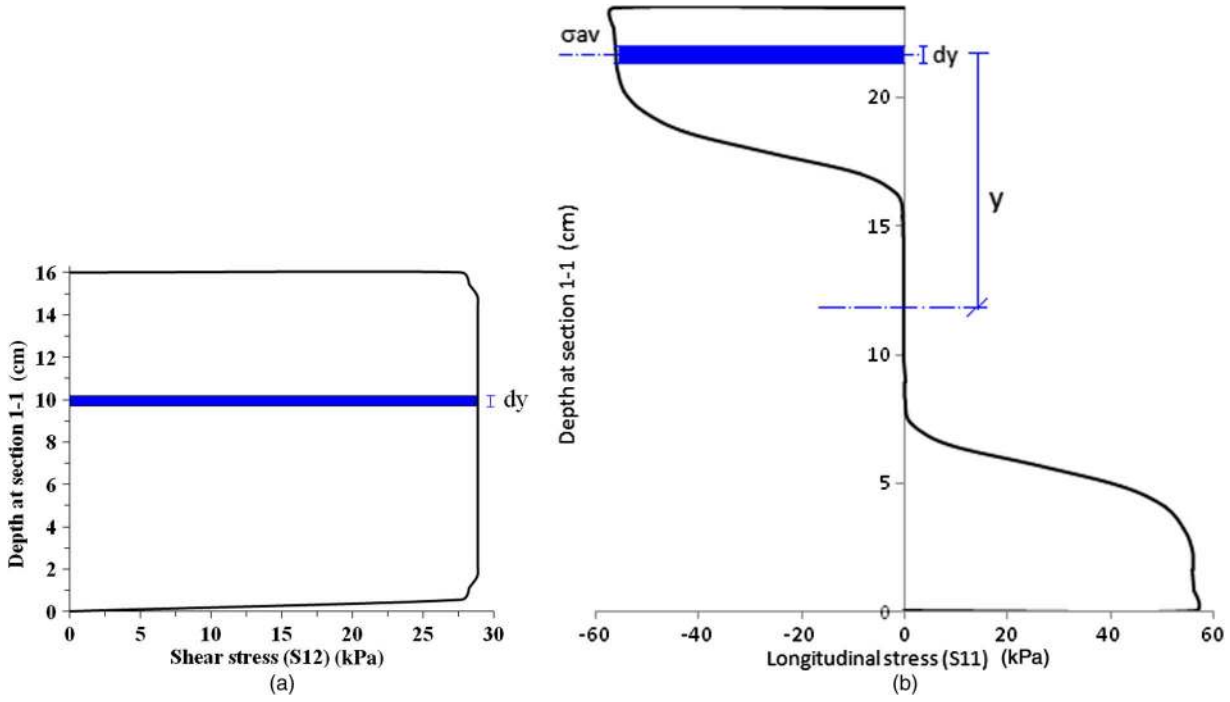

Fig. 11. Stress distribution: (a) shear stress at section A-A; (b) longitudinal stress at section B-B

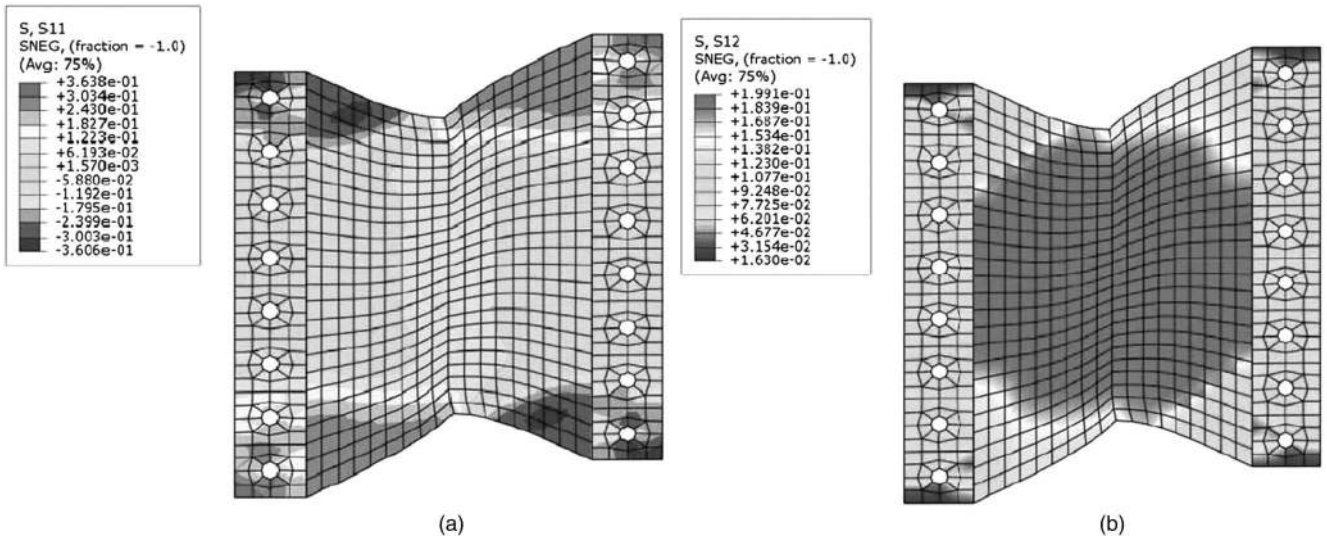

Fig. 12. Stresses for the restrained steel plate shear link at a total link rotation of 0.13 rad: (a) longitudinal stresses; (b) shear stresses

$$V_{Dt} = \frac{4M_P}{H_{\text{tot}}} + n\sigma_y A_b \sin\theta\left(\frac{L}{H_{\text{tot}}}\right) \tag{19}$$

in which n = number of BRBs; A_b = cross section area of the yielding portion of the BRB; and σ_y = yield strength of the BRB.

Similarly to the case of SPSLs, it can be seen that the first term of the equation represents the maximum bare frame shear strength, from which it is concluded that the contribution of the BRBs to the maximum shear strength, V_{DS}, is the second term of the equation.

The elastic contribution of the BRBs to the total elastic lateral stiffness of the system can be calculated by dividing the contribution of the BRBs to the maximum shear strength, V_{DS}, by the top horizontal displacement that corresponds to the onset of BRB yielding, and can be calculated as:

$$K_b = \frac{nEA_bLH\sin\theta\cos\theta}{L_{ysc}H_{\text{tot}}^2} \tag{20}$$

The base shear of the structural fuse system at the onset of column yielding can be obtained by replacing M_p by M_y in the predeeding equations. The adequacy of these simple equations for design is assessed in a subsequent section. More details on the development of the previous equations are addressed in El-Bahey and Bruneau (2010).

Finite-Element Modeling

A preliminary finite-element analysis was conducted to validate the SPSL concept proposed previously. This was deemed necessary to develop some confidence that the newly proposed system could work as expected, and that yielding would occur in pure shear in the middle part of the SPSL (and that pure flexure yielding would develop simultaneously in the wedge parts for the case of a balanced link edge angle SPSL). This also was done to better quantify

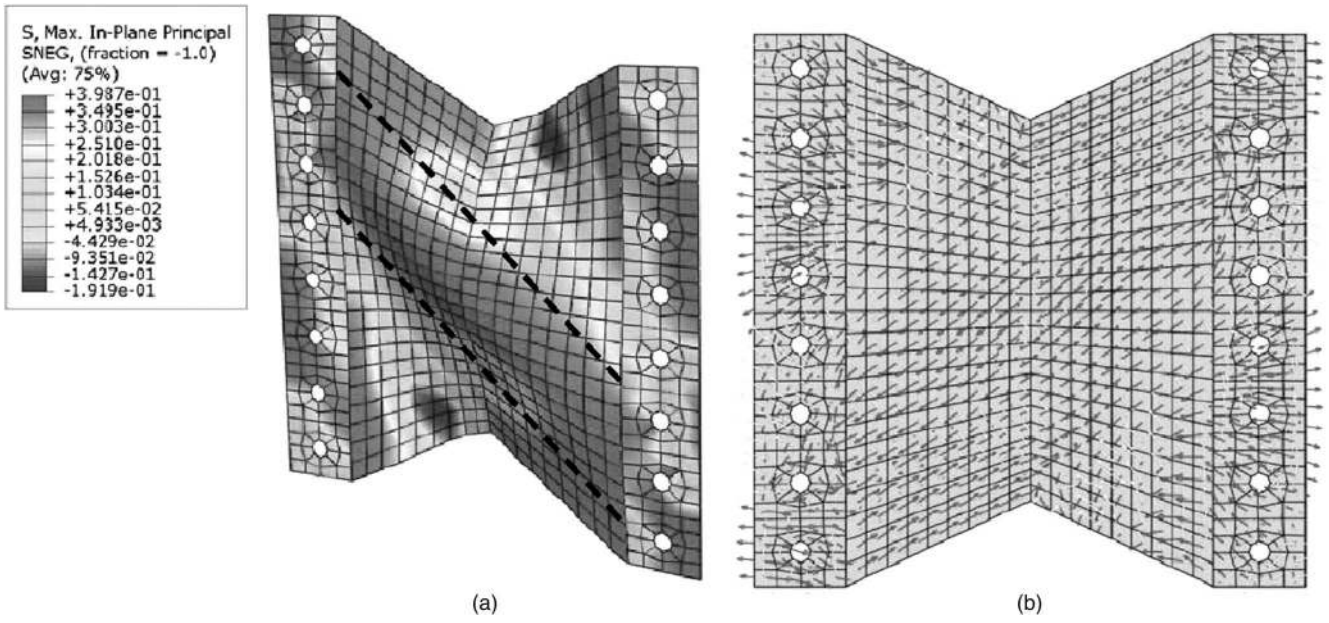

Fig. 13. Unrestrained steel plate shear link at a total link rotation of 0.13 rad: (a) maximum in-plane principle stresses; (b) principle stresses orientation

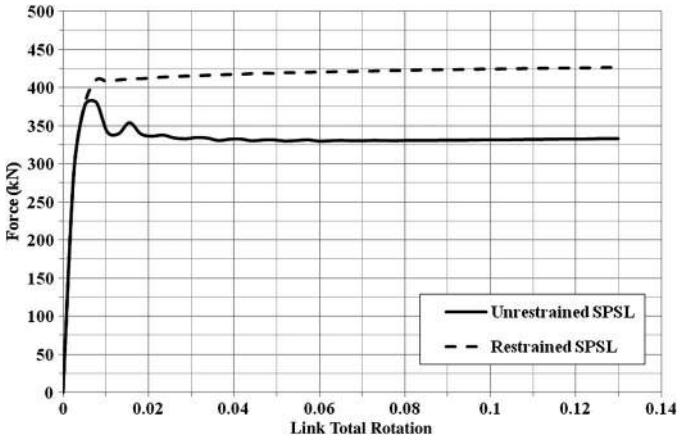

Fig. 14. Comparison between strengths of restrained and unrestrained steel plate shear links

the width of the tension field strip that is expected to develop for the case of the unrestrained SPSL.

Two finite-element models have been developed, both possessing exactly the same dimensions and with a balanced link edge angle. The first was restrained against lateral buckling (i.e., no lateral displacement movement was allowed during the analysis), whereas the second was free to move in the lateral direction and consequently buckle.

Geometry of the models was chosen to satisfy the proposed equations, which resulted in a SPSL of y_0 equal to 412 mm, and a link length, e, equal to 400 mm. The link edge angle, θ, was chosen to be equal to θ_b; which is approximately 25°. A thickness of 5 mm was chosen for the analysis, which is the same thickness that was chosen for the experimental specimens (El-Bahey and Bruneau 2011). An elasto-perfectly plastic material of yield strength equal to 350 MPa (50 ksi) was chosen to validate the proposed equations for calculating the plastic moment and plastic shear of the SPSLs. The von Misses yield criteria was chosen to define the plastic behavior of the link, as commonly done for steel. Poisson's ratio was assumed to be equal to 0.3, which is typical for structural grade steel. Loading was applied for both models as a vertical monotonic displacement up to a total rotation of 0.13 rad, which was an arbitrarily chosen value, at which it was decided to stop the analysis.

Longitudinal and shear stress plots were developed at sections A-A and B-B shown in Fig. 4 for the restrained SPSL. The maximum shear strength observed can be calculated by integrating the shear stress plot at section A-A. The value of the maximum shear force that was calculated from integration is 405 kN, and also can be seen in Fig. 11(a); the theoretical value of the plastic shear force calculated using Eq. (5) was found to be equal to 397 kN. The corresponding value of the plastic moment reduced by the presence of large shear stresses at the ends of the links (section B-B) was calculated by integrating the longitudinal stress plot in Fig. 11(b) as 80 kN/m, compared to 79 kN/m calculated by using Eq. (4). Contour plots for the longitudinal and shear stresses at a total link rotation of 0.13 rad are shown in Fig. 12. It can be seen from the plots that pure shear yielding is occurring in the middle part of the SPSL, whereas pure flexural yielding is occurring in the wedge parts.

For the unrestrained SPSL, the load increases with respect to the total link rotation and the SPSLs behaves similarly to the restrained SPSL until the geometric nonlinearities force the SPSL to buckle out-of-plane, at which point a drop of strength is observed (at 0.004 rad in that particular example) and the SPSL starts yielding

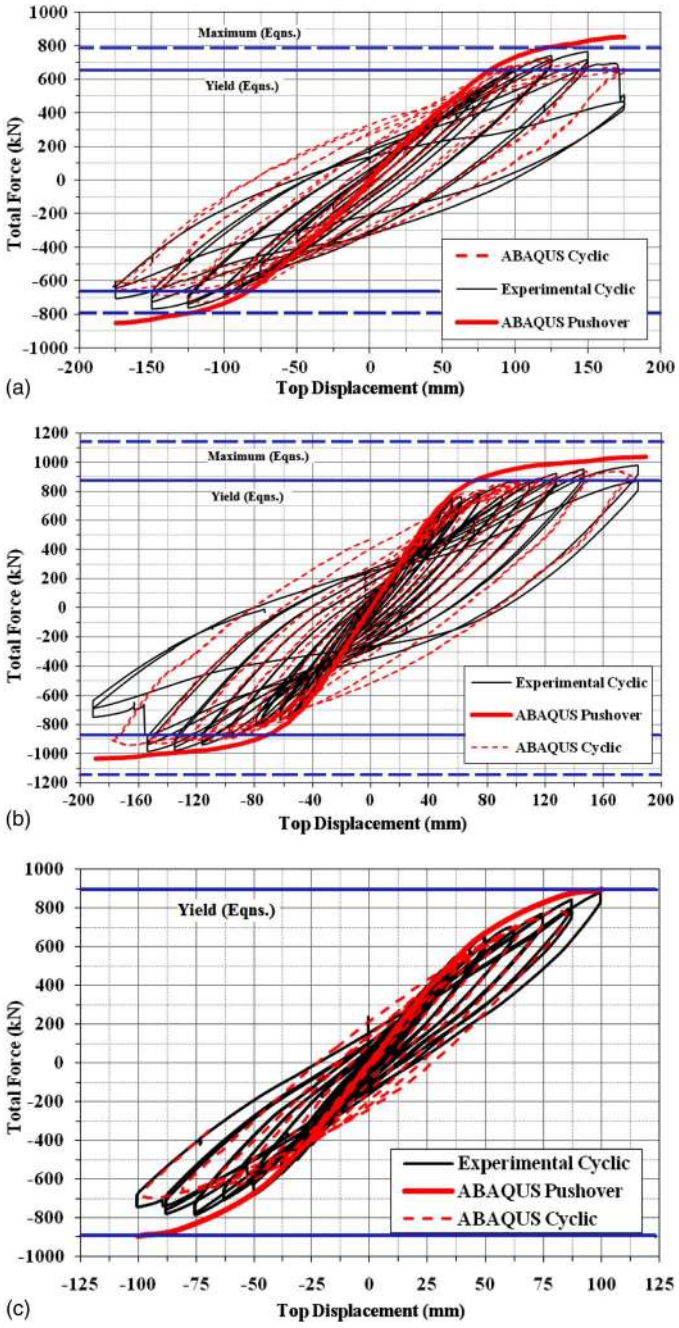

Fig. 15. Comparison between experimental and analytical results: (a) S2-2; (b) S1; (c) S2-1

by tension field action. Depending on the magnitude of initial imperfection introduced in the analysis, and for large plate slenderness, the peak value typically would not occur, as the plate would transition "smoothly" into its buckled and diagonal tension mode (e.g., Vian and Bruneau 2005). Fig. 13 shows the principal stress distribution for the unrestrained SPSL at a total link rotation of 0.13 rad. A tension field strip is observed in the figure with a strip width of approximately 1/3 the SPSL diagonal length, D, from which the unrestrained SPSL shear force value after buckling occurs, can be calculated as:

$$V_{\max} = \sigma_y t S \sin \alpha \tag{21}$$

in which S is calculated from the finite-element model as equal to $1/3D$; and the strip is inclined with an angle α equal to approximately 55°.

Table 1. Summary of Peak Results

Specimen	Elastic stiffness (kN/mm) (Exp.)	Elastic stiffness (kN/mm) (Eq.)	Base shear at column yielding (kN) (Exp.)	Base shear at column yielding (kN) (Eqn.)	Base shear at column yielding (kN) (finite-element model-Pushover)	Base shear at column yielding (kN) (finite-element model-Cyclic)	Max. base shear (kN) (Exp.)	Max. base shear (kN) (finite-element model-Cyclic)	Max. base shear (kN) (Eqn.)	Fuse ductility at column yielding (Exp.)	Column yielding drift (%) (Exp.)	Max. drift (%) (Exp.)	Strength reduction at max. drift (%) (Exp.)
S1 (Unrest.)	22	24	875	880	950	880	982	980	1133	4	1.6	3.3	33
S1 (rest.)	22	22	—	960	1150	1100	—	1150	1243	—	—	—	—
S2-1	21.5	32	881	899	900	885	—	—	1149	4	1.6	—	—
S2-2	8	9.7	666	657	740	670	770	760	788	—	1.6	4.3	29

From Eq. (21), the value of the unrestrained SPSL force is found to be equal to 347 kN compared to 330 kN observed from a push-over curve shown in Fig. 14. This value is about 80% of the total strength obtained if the link is restrained against out-of-plane buckling.

Finite-element models replicating the behavior of all systems tested in El-Bahey and Bruneau (2011) were developed using the ABAQUS/explicit software. First, a model was developed to replicate the observed experimental behavior of the bare frame composite columns (Specimen S2-2). The structural fuses elements were then added to replicate behavior of the bents by using SPSLs (Specimen S1) or BRBs as structural fuses (Specimen S2-1).

For the composite columns, S4R shell elements were used to model the steel box, whereas C3D8R brick elements were used for the infill concrete and the cap beam. To model the interaction between the steel and the concrete, a surface-to-surface contact option was used to replicate the contact condition between both surfaces, to allow normal separation, and to capture buckling of the steel when it develops. A contact interaction property can define tangential behavior (friction and elastic slip) and normal behavior (hard, soft, or damped contact and separation). The tangential behavior was chosen by using a friction model that defines the force resisting the relative tangential motion of the surfaces in a mechanical contact analysis. The coefficient of friction between steel and concrete was arbitrarily taken as 0.35, as multiple analyses conducted to investigate the sensitivity of changing this parameter showed that it had no significant effect on the global behavior of the model over a range of values that seemed reasonable (from 0.25 to 0.5); the chosen value was selected for convenience. The behavior in the direction normal to the steel-concrete interface was defined by using the hard contact pressure-overclosure relationship.

The material nonlinearity for the steel columns was defined by using the nonlinear combined kinematic/isotropic hardening plasticity model available in ABAQUS. The von Misses yield criteria was chosen to define the plastic behavior of the link, which is suitable for ductile materials such as steel. Poisson's ratio was assumed to be equal to 0.3 which is typical for structural grade steel. For the analyses, the properties of the A572 Gr.50 steel that was used for the columns were taken from coupon tests. A concrete damaged plasticity model in ABAQUS was used to simulate the behavior of concrete infill. This model is on the basis of the models proposed by Lubliner et al. (1989) and Lee and Fenves (1998). The model defined in ABAQUS is a continuum plasticity-based damage concrete model that assumes two main failure mechanisms; tensile cracking, and compressive crushing of the concrete material, for which the uniaxial tensile and compressive response of concrete is characterized by damaged plasticity.

Boundary conditions were specified by restraining all the nodes at the base of the columns, replicating a fixed end condition. Two types of loading conditions were defined and applied to a reference point located on one edge of the rigid cap. The first was a monotonic pushover displacement, and the second was a cyclic displacement protocol replicating the conditions in the experimental investigation. Meshes were generated on the merged model after "seeding" every edge by specifying the number of elements desired along that edge. The models were meshed entirely using quadrilateral elements.

The modeling assumptions, used in the analysis of the bare frame with composite columns (to replicate the behavior of Specimen S2-2), also were used in all subsequent analyses because the composite columns were parts of the structural fuse systems considered.

Specimen S1

For specimen S1, that has SPSLs as structural fuses, two ABAQUS models where conducted: the first model represents the experiments performed for the SPSLs without lateral restraints; the second model represents the incomplete testing performed on the SPSLs with the presence of the lateral restraints.

For both models, 3D deformable planar shell elements were used to model the SPSLs. The only difference between the two models constructed for this specimen is that, in one case, the SPSLs were restrained from out-of-plane motion by imposing a boundary condition of zero displacement in the out-of-plane direction.

Specimen S2-1

For specimen S2-1, that has BRBs as structural fuses, three dimensional deformable axial members (wire elements) were used to model the BRBs. The gusset plates to which the BRB connected were not modeled; therefore, some stress concentration attributable to the "point load" effect of connecting the BRBs to single nodes in the steel was expected. Nevertheless, these few points of fictitiously high stress concentration were not expected to affect the global system behavior.

Comparison with Experimental Results

Fig. 15 shows a comparison between the experimental data, the ABAQUS cyclic analysis, ABAQUS pushover analysis, and the values corresponding to the maximum and yield base shear of the columns computed by using the equations developed previouslly, for all tested specimens. Table 1 summarizes the results of this comparison with respect to elastic stiffness and base shear of the specimens. Both the experimental and finite-element cyclic data match well for all specimens, as the entire peak base shear values were captured along with the strength and stiffness degradation of the specimen that occurred owing to the local buckling of the columns. The values obtained using the proposed simple equations match well with the experimental results at the yield base shear level, whereas it overestimates the strength by an average value of 13% at the maximum base shear level. This is attributed to the fact that at the maximum base shear level, the full theoretical plastic moment is considered in calculating the corresponding base shear, whereas in the actual case, the maximum moment developed at the base of the columns is slightly less than the theoretical plastic moment attributable to the development of local buckling in the columns. Overall, the simple design equations obtained from free-body diagrams give good estimates of both the stiffness and the base shear compared to the FEM and the experimental data.

The pushover analysis gives slightly higher results than that of the cyclic analysis; this is attributed to the fact that the local buckling in the composite columns does not develop as easily during a

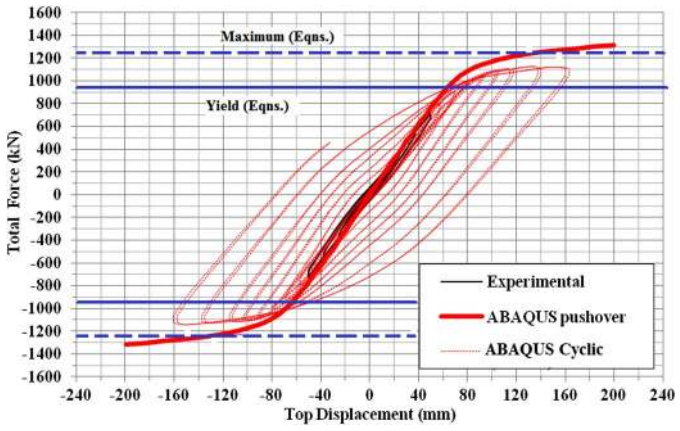

Fig. 16. Comparison between experimental and analytical results for specimen S1 (test 1)

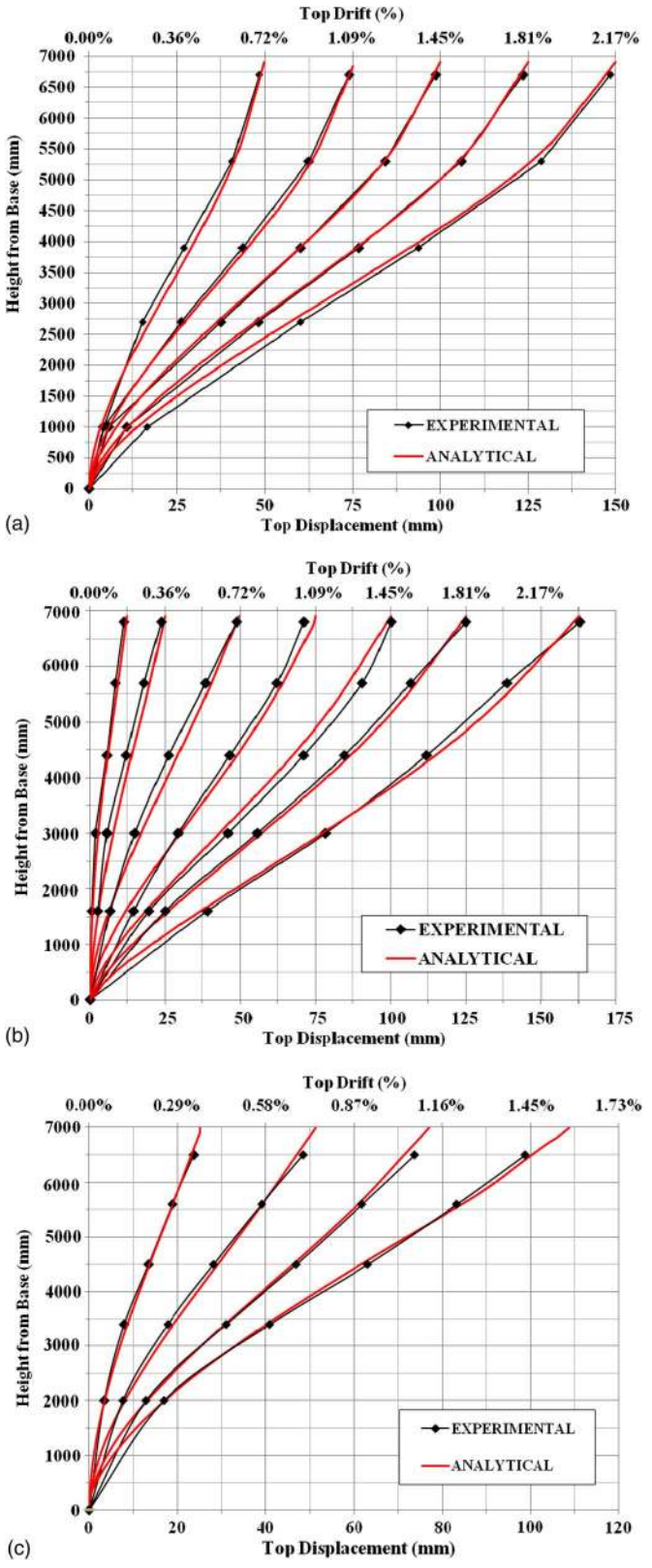

Fig. 17. Comparison between the deflected shapes of columns at various drift levels: (a) S2-2; (b) S1; (c) S2-1

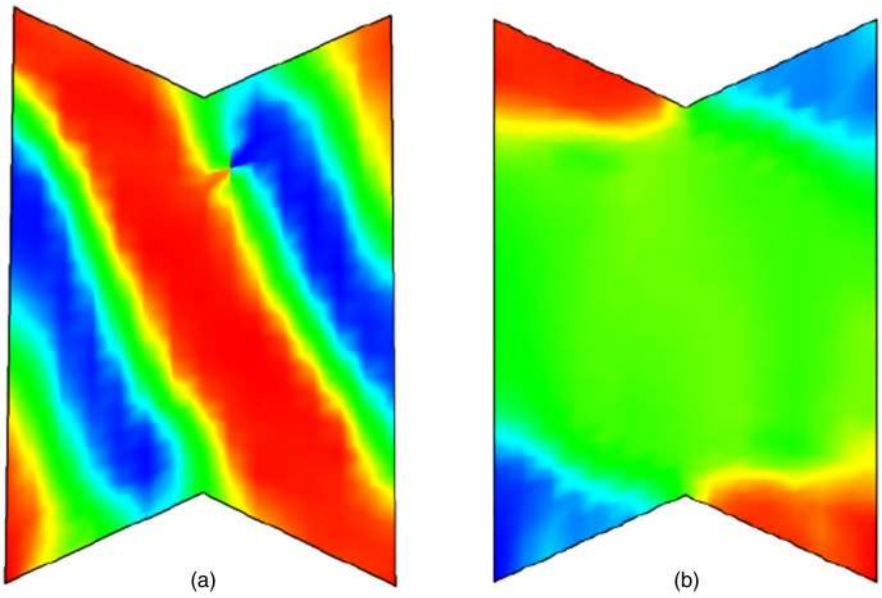

Fig. 18. Maximum in-plane principal stresses at 175 mm top displacement (2.5% drift) for specimen S1: (a) unrestrained steel plate shear link; (b) restrained steel plate shear link

pushover analysis because the faces of the composite box columns that are subjected to monotonic tension only stretch (i.e., they are not subjected to the reversed loading under which these longer members would be easier to buckle), and the faces in compression can only develop local buckling if crushing starts to develop in the concrete infill. Under cyclic loading condition, local buckling can develop in both faces owing to the fact that the stretched steel plates become longer and thus easier to buckle when compressed after being stretched (even if concrete was infinitely rigid and strong in compression).

Fig. 16 shows a comparison between the experimental results, computational results, and the values corresponding to the maximum and yield base shear of the columns computed by using the equations developed previously for the uncompleted test for specimen S1 (Test 1) that has laterally restrained SPSLs.

It was unfortunate that the experimental testing of test 1 was terminated at a top displacement of 50 mm (0.72% drift) because of a sudden weld failure at one of the bottom splices as described in the companion paper. Nevertheless, the comparison between the analytical models and experimental results for the previous tests gave confidence about the accuracy of the analytical model, and the analytically predicted behavior of the frame with the laterally restrained SPSLs calculated using the ABAQUS model as if the entire cyclic history had been applied to that case, for informational purposes. The same observations regarding the accuracy of the simple plastic analysis equations are possible in this case. Obviously, that extrapolation is speculative and not verified by experimental results at this stage; however, further experimental testing is underway for laterally restrained SPSL that investigates the conditions under which this behavior could have been obtained.

Fig. 17 shows a comparison between the experimental data obtained for the deflected shape of the columns versus the ABAQUS analytical results for all specimens. The experimental data were obtained using the 5 string potentiometers located at different heights from the top of the foundation. The analytical and experimental results match well. A double curvature behavior with an inflection point at about $1/3$ height from the base is observed for specimen S2-2; indicating that the two twin columns behaves as a frame with bending moments developing more at the bottom than the top of the columns. For specimens S1, and S2-1, the columns behave differently before and after yielding of the fuses. Before the fuses yield, the entire pier consisting of the two columns and the fuses behave as one vertical cantilever member, with the columns being the flanges of that member, and the fuses being its web. Therefore, a single-curvature behavior is observed for the system up to the point where the fuses start to yield at about 32 mm top displacement (0.46% drift); thereafter, the columns behave individually as two columns in a frame and a double curvature develops.

Fig. 18 shows the in-plane principal stresses for SPSL at 175 mm top displacement (2.5% drift). A tension field strip develops along the diagonal of the SPSL with a width of about 228 mm (9 in.), and an angle of 55° to the horizontal for the case of unrestrained SPSLs. Further investigation, looking at the stress vectors, actually reveals a diagonal tension field acting at 45° in the middle of the plate (showing the dominance of pure shear yielding), and stresses reorienting to remain parallel to the plate edges near those edges, in which shear and flexure combine. By comparison, for the case of restrained SPSLs, pure shear yielding can be seen in the middle part of the link, whereas pure flexural yielding is observed in the top and bottom of the links as shown in the figure.

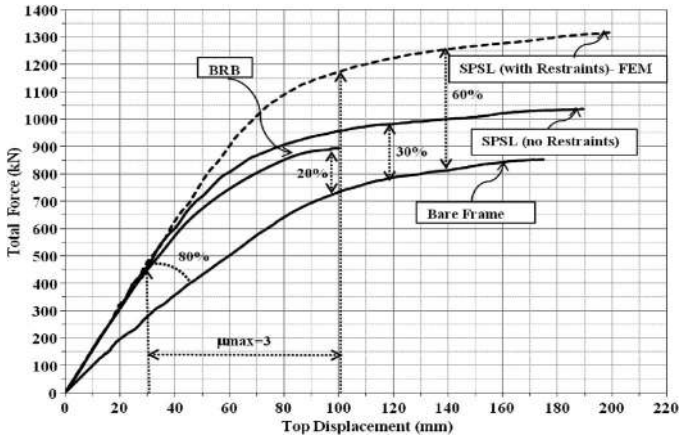

Fig. 19. Pushover results comparison for all specimens

Fig. 19 shows the pushover results comparison for all specimens. A stiffness increase of 80% is observed between the bare frame (specimen S2-2) and the frame with the structural fuses inserted between the columns. A 30% strength increase also is observed between Specimen S2-2 and Specimen S1, whereas a 20% increase is observed between Specimen S2-2 and Specimen S2-1. A 60% strength increase would have been expected if the lateral restraints had been left in place for the test, from which it is concluded that, the lateral restraints can be substantially effective to increase strength. However, for the structural fuse concept, increases in strength and stiffness are parameters that can be varied at will by the designer.

Conclusion

The structural fuse concept for bridges has been investigated and validated through an experimental project for a 2/3 scale proposed twin column bridge pier bent concept using SPSLs and BRBs as a series of structural fuses in a companion paper. Here, an analytical investigation has been conducted to replicate the full range of results obtained from the experiments and to highlight the differences in behavior among all tested specimens. Design equations for the proposed system were presented and compared to the results obtained from the analytical and experimental investigation. It was found that the results obtained from the ABAQUS model correctly match both the experimental and the numerical equations.

Acknowledgments

This research was supported in part by the Federal Highway Administration under contract number DTFH61-07-C-00020 to Multidisciplinary Center for Earthquake Engineering Research (MCEER). Donation of the bisteel panels by Corus Bisteel and the BRBS by Star Seismic is also sincerely appreciated. However, any opinions, findings, conclusions, and recommendations presented in this paper are those of the authors and do not necessarily reflect the views of the sponsors.

References

ASCE. (1971). "Plastic design in steel, a guide and commentary." *ASCE manuals and reports on engineering practice, No. 41*.

Berman, J. W., and Bruneau, M. (2005). "Approaches for the seismic retrofit of braced steel bridge piers and proof-of-concept testing of a laterally stable eccentrically braced frame." *Tech. Rep. MCEER-05-0004*, Multidisciplinary Center for Earthquake Engineering Research, Buffalo, NY, 4.

El-Bahey, S., and Bruneau, M. (2010). "Analytical development and experimental validation of a structural-fuse bridge pier concept." *Tech. Rep. MCEER-10-0005*, Multidisciplinary Center for Earthquake Engineering Research, Buffalo, NY.

El-Bahey, S., and Bruneau, M. (2012). "Bridge piers with structural fuses and bi-steel columns. I: Experimental testing." *J. Bridge Eng.*, 17(1), 25–35.

Engelhardt, M. D., and Popov, E. P. (1989). "Behavior of long links in eccentrically braced frames." *Rep. No. UCB/EERC-89*, Earthquake Engineering Research Center, University of California, 1.

Hibbitt, Karlsson, and Sorenson, Inc. (HKS). (2005). *ABAQUS/CAE user's manual version 6.5-1*, Hibbitt, Karlsson, and Sorenson, Inc., Pawtucket, RI.

Kasai, K., and Popov, E. (1986a). "Cyclic web buckling control for shear link beams." *J. Struct. Eng.*, 112(3), 505–523.

Kasai, K., and Popov, E. (1986b). "General behavior of WF steel shear link beams." *J. Struct. Eng.*, 112(2), 362–382.

Lee, J., and Fenves, G. L. (1998). "Plastic-damage model for cyclic loading of concrete structures." *J. Eng. Mech.*, 124(8)892.

Lubliner, J., Oliver, J., Oller, S., and Onate, E. (1989). "A plastic-damage model for concrete." *Int. J. Solids Struct.*, 25(3), 299–326.

Vian, D., and Bruneau, M. (2005). "Steel plate walls for seismic design and retrofit of building structures." *Tech. Rep. MCEER-05-0010*, Multidisciplinary Center for Earthquake Engineering Research, State Univ. of NY at Buffalo, NY.